Numerical and Analytical Modelling of Sandface Temperature in a Dry Gas Producing Well

Accepted Manuscript

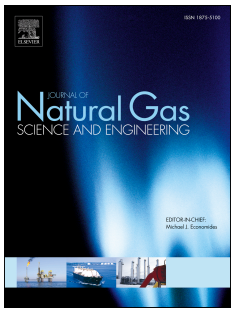

Numerical and analytical modelling of sandface temperature in a dry gas producing well

Akindolu Dada, Khafiz Muradov, Kokou Dadzie, David Davies

PII: S1875-5100(17)30050-1

DOI: 10.1016/j.jngse.2017.02.005

Reference: JNGSE 2058

To appear in: *Journal of Natural Gas Science and Engineering*

Received Date: 4 October 2016

Revised Date: 26 January 2017

Accepted Date: 1 February 2017

Please cite this article as: Dada, A., Muradov, K., Dadzie, K., Davies, D., Numerical and analytical modelling of sandface temperature in a dry gas producing well, *Journal of Natural Gas Science & Engineering* (2017), doi: 10.1016/j.jngse.2017.02.005.

Numerical and Analytical Modelling of Sandface Temperature in a Dry Gas Producing Well

Akindolu Dada[a,*], Khafiz Muradov[a], Kokou Dadzie[b], David Davies[a]

[a] *Institute of Petroleum Engineering, Heriot-Watt University*
[b] *School of Engineering and Physical Sciences, Heriot-Watt University*

Abstract

The oil and gas reservoir pressure response to the changes in the fluid production rate has been traditionally used to estimate the reservoir properties. Numerous analytical and numerical models have been developed to describe the transient pressure in and around a production well so as to interpret the in-well pressure measurements. Pressure Transient Analysis (PTA) is routinely used by Production and Reservoir Engineers at various stages in a wells life; initially for reservoir characterisation and, later, for well performance monitoring and (wider) reservoir surveillance. The recent application of high precision, downhole, temperature sensors has resulted in PTA being complemented by Temperature Transient Analysis (TTA). Recent TTA research has shown that comprehensive information on the state of the near-wellbore zone and fluid flow rates and composition can potentially be derived from such measurements. However, the derivation of useable TTA solutions describing the mass and energy transfer in porous media is challenging since it is necessary to simultaneously account for both the thermodynamic and the transient transfer effects. This paper reports a step in the development of a novel Temperature Transient Analysis (TTA) workflow. This is the first publication, to our knowledge, where the gas production TTA solutions, properly accounting for the compressible gas nature, are presented and discussed. A numerical model for determining sandface tran-

*Corresponding author
Email address: aod30@hw.ac.uk (Akindolu Dada)

sient temperature in a dry gas producing well is developed. Simulations studies are run to understand the physics of transient temperature change and to make realistic assumptions to simplify the analytical model so as to derive an early-time, analytical solution. Finally, the limitations of the developed analytical solution are presented. This work is an important step towards a comprehensive PTA/TTA data analysis framework for multi-phase production wells.

Keywords: Temperature transient analysis, Analytical solution, Non-isothermal flow in porous media, Compressible fluids, Intelligent well

---

List of Symbols

Variables

β	Non-Darcy coefficient
β_T	Thermal expansion coefficient
ε	Joule-Thomson coefficient
η	Adiabatic coefficient
η^*	Formation averaged adiabatic coefficient
μ	Viscosity of fluid
ρ	Density of fluid
ρ_r	Density of rock
ϕ	Porosity
ψ	Pseudo-pressure
ψ_i	Pseudo-pressure at initial conditions
c	Ratio of gas heat capacity to averaged formation heat capacity
d	molal density
γ	Euler-Mascheroni constant
k	Permeability
r	Radius
r_{nD}	Ratio of non-Darcy pressure drop to Darcy pressure drop component
r_T	Thermal radius of investigation
t	Time

$\boldsymbol{v}$	Velocity
A	Constant term in pressure pseudo-pressure relationship
B	Coefficient in pressure pseudo-pressure relationship
C_p	Specific heat capacity of fluid
C_{pr}	Specific heat capacity of rock
C_t	Total formation compressibility
P	Pressure
Q_d	Dimensionless pressure
T	Temperature
T_{nD}	Ratio of non-Darcy temperature change due to Darcy temperature change

Subscripts

$crit$	Critical condition
i	Initial conditions
r	Rock
t	Time
sc	Surface conditions
T	Thermal
w	Well
w	Wellbore
wf	Well flowing

1. Introduction

. The business-pull for Temperature Transient Analysis (TTA) research has increased in recent years due to the introduction and wide spread application of sensors of sufficient sensitivity that can detect the small temperature changes associated with TTA. The development of a comprehensive PTA/TTA data analysis framework will allow the full Added Value to be reaped from providing the measured data to the engineers desk-top in real-time. Reliable real-time

reservoir monitoring and management, in its turn, is a long-awaited goal able to make a notable difference to the efficiency and impact of hydrocarbon production.

. The development and application of TTA solutions for flow rate allocation in oil wells has been reported as early as 2012 by Muradov and Davies (2012b) for horizontal wells and Ramazanov et al. (2010) for vertical wells. Transient temperature was also numerically proven to be able to estimate the formation parameters (Sui et al., 2010; Duru and Horne, 2010) as well as to determine the length of a hydraulic fracture (App, 2013). The application of the TTA workflow description by Muradov and Davies (2012b) was later illustrated by examples using real-well data (Muradov and Davies, 2012b, 2013). The combination of TTA and PTA allows the full reconstruction of zonal reservoir properties and flow rates after a small fraction of the complete transient period has elapsed.

. TTA requires a comprehensive model of heat and mass transfer in porous media. Bird et al. (2007) proposed a thermal model which has been adapted for porous media flow; allowing analytical and numerical liquid solutions based on this or similar models to be obtained by Muradov and Davies (2012a), Duru and Horne (2010), Ramazanov et al. (2010) etc. Predicted temperatures derived from these thermal models were successfully compared to real-well data by Muradov and Davies (2013) and Duru and Horne (2010).

. Most of the work done in the area of transient sandface temperature modelling has been limited to slightly compressible fluids (i.e. liquids). This limitation allowed the introduction of simplifying assumptions to the thermal models. However, extending their application to gasses (i.e. compressible fluids) results in a highly non-linear mathematical problem which is more difficult to solve. This explains why there are only a few publications on TTA for gas producing wells. For example, Sui et al. (2010) coupled a wellbore model to a numerical, multilayer, gas reservoir model. They used transient temperature data from the forward model to determine the layer permeability and skin properties. The

inversion of the forward model was accomplished by running multiple numerical simulations and minimizing the objective function by nonlinear regression.

. Numerical inversion solvers have the capability to solve many inverse problems. However, these methods do not provide the valuable insights into the problem that an analytical model provides. Analytical solutions have the additional advantage of providing a unique solution more quickly, and with reduced computational resources, than is required by the numerical approach to solving an inverse problem. This work develops analytical models for prediction of downhole transient sandface temperatures of gas producing wells. It forms one step in the development of a comprehensive TTA workflow.

2. Governing Equations

Flow in porous media is usually described by combining the empirical Darcys law equation (Eq. 1) with the continuity equation (Eq. 2), this would give the diffusivity equation (Eq. 3):

$$\boldsymbol{v} = -\frac{\boldsymbol{K}}{\mu}\nabla P \tag{1}$$

$$\frac{\partial}{\partial t}(\phi\rho) + \nabla\cdot(\rho\boldsymbol{v}) = 0 \tag{2}$$

$$\frac{\partial}{\partial t}(\phi\rho) + \nabla\cdot\left(-\rho\frac{\boldsymbol{K}}{\mu}\nabla P\right) = 0 \tag{3}$$

Using an appropriate equation of state (EOS) to express density as a function of pressure (e.g. $\rho = \frac{P}{ZRT}$), Eq. 3 can be expressed explicitly as a function of pressure.

$$\frac{\partial}{\partial t}\left(\phi\frac{P}{ZRT}\right) + \nabla\cdot\left(-\frac{P}{ZRT}\frac{\boldsymbol{K}}{\mu}\nabla P\right) = 0 \tag{4}$$

Where $\boldsymbol{v}$ is the flow velocity, ρ is the density, ϕ is the porosity, P is the pressure, μ is the viscosity, R is the specific gas constant, T is the temperature, Z is the gas compressibility factor and $\boldsymbol{K}$ is the permeability tensor.

Eq. 4, the basic diffusivity equation used to calculate pressure, can be solved by numerical methods. However, the flow behaviour departs from the Darcys law at high flow velocities. Geertsma (1974) provided the limits for applying Darcys law in gas and high rate oil wells.

Traditionally used analytical pressure solutions assume that Darcys Law, with its laminar flow assumption, is valid. We will not initially include the non-Darcy (inertial) effects in the numerical simulations. This will ensure consistency with the assumptions behind our analytical solutions. We will then define the boundaries of the region in which non-Darcy effects can be neglected in a later section.

2.1. Thermal Model

The numerical thermal model used (Eq. 5) was proposed by Sui et al. (2008). It includes temperature changes in porous media due to transient fluid expansion, Joule-Thomson effect, heat conduction and convection:

$$\begin{aligned} &\overline{\rho C_p}\frac{\partial T}{\partial t} - \phi\beta_T T\frac{\partial P}{\partial t} - \phi C_f\left(P + \rho_r C_{pr} T\right)\frac{\partial P}{\partial t} \\ &= -\rho \boldsymbol{v} C_P \cdot \nabla T + \beta_T T \boldsymbol{v} \cdot \nabla P - \boldsymbol{v} \cdot \nabla P + K_T \nabla^2 T \end{aligned} \tag{5}$$

Where: C_p and C_{pr} are the specific heat capacity of the gas and formation rock respectively, ρ_r is the density of the formation rock, C_f is the formation compressibility, $\boldsymbol{v}$ is velocity, β_T is the thermal expansion coefficient, K_T is the thermal conductivity, T is the temperature and $\overline{\rho C_p}$ is the mean formation heat capacity.

3. Numerical Modelling

OpenFOAM, an open source library for numerical simulations in continuum mechanics using the finite volume method, was chosen for this work. Using an open-source library makes it possible to modify existing solvers or create new solvers which use existing library components listed in Jasak et al. (2007). OpenFOAM provides the flexibility needed.

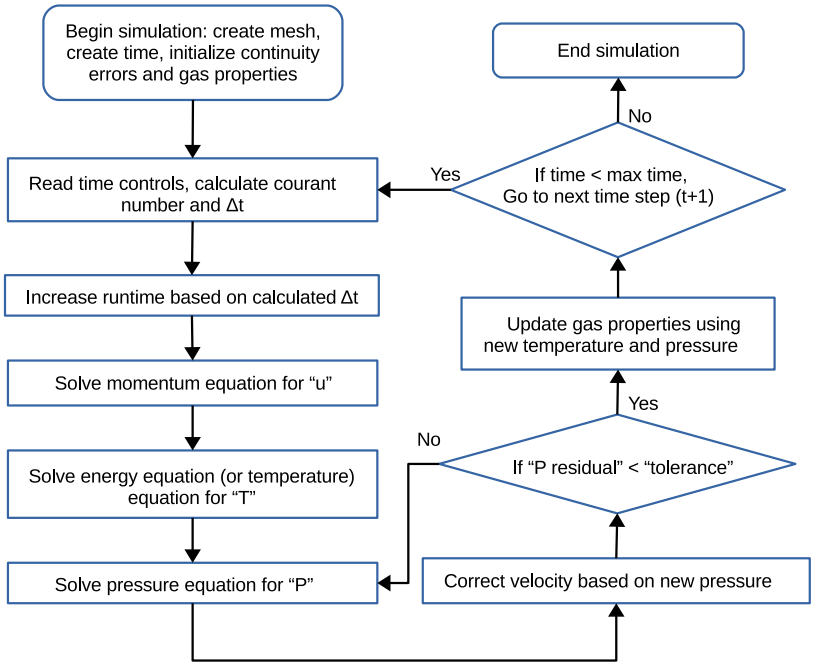

Figure 1: Flowchart for numerical simulation

3.1. Solver Modification

An existing solver "rhoPimpleFoam" (OpenCFD, 2014), -originally designed to simulate transient laminar or turbulent flow of compressible fluids- was customized to simulate transient compressible flow in porous media as follows:

1. Adding the ability to read gas property tables allows the inclusion of the actual pressure-temperature dependence for different gas properties (see Appendix A for details of gas properties used).
2. Changing the momentum equation to Darcys Equation (Eq. 1).
3. Modifying the continuity equation for porous media flow (Eq. 2).
4. Altering the energy equation to the thermal model (Eq. 5) published by Sui et al. (2008).

An auxiliary library, swak4foam, is used alongside OpenFOAM to set the variable properties for each element in the mesh. Fig. 1 is a flowchart of the

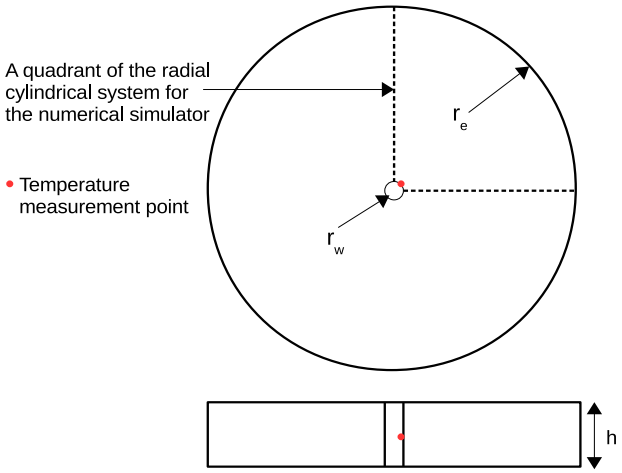

Figure 2: Radial cylindrical system, showing quadrant for numerical simulation and measurement probe location

solution procedure followed by our solver.

3.2. Simulation Setup

A quarter symmetry element of a cylindrical numerical simulation model of a vertical, open-hole wellbore situated in the centre of a circular, horizontal reservoir was prepared (Fig. 2). The numerical mesh employed grid refinement in the radial direction near the wellbore, since the transient effect is greatest in the near-wellbore region. The gridding was prepared using OpenFOAMs simpleGrading method. This method employs a uniform expansion ratio that is based on the ratio between the first to the last element lengths (the well radius and the boundary radius respectively). The expansion ratio is calculated from Eq. 6

$$ER = \frac{el_1}{el_n} \tag{6}$$

$$L = r_e - r_w = \sum_{i=1}^{n} el_i = \frac{el_1\,(1-\varepsilon^n)}{(1-\varepsilon)} \tag{7}$$

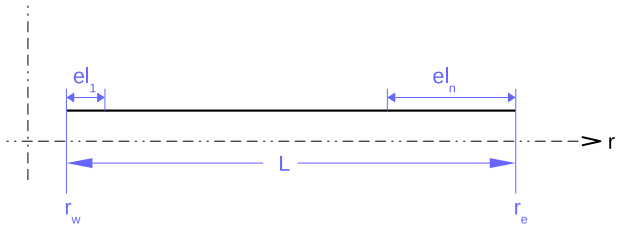

Figure 3: Radial direction showing first and last element lengths

$$el_i = el_1\left(\varepsilon^{i-1}\right) \tag{8}$$

Where n is number of radial mesh elements, L is the radial length, r_e is the exterior radius of reservoir boundary, r_w is the well radius, el_i is the radial length of the i^{th} element.

$$\varepsilon = \frac{el_{i+1}}{el_i} \tag{9}$$

The model was divided into 40 grid blocks in the z-direction. Only radial fluid flow is considered in the model. A vertical, geothermal gradient of 0.025K/m was imposed across the model, allowing heat conduction to occur in this direction. Heat exchange with the underlying and overlying formations was not modelled. We assumed that it has a negligible impact at early times, as observed by Muradov and Davies (2012a).

Most, if not all, gas reservoirs have a temperature greater than the critical temperature for the chosen natural gas composition. The fluid will thus exist purely in the gaseous state regardless of the reservoir pressure. Appendix (A) lists the gas property equations and correlations used. The density of a gas is a function of the pressure (Eq. 10) while Eq. 11 gives the gas hydrostatic head at the bottom of the reservoir and Eq. 12 is the relative magnitude of hydrostatic head to the reservoir pressure. A reservoir thickness of about 200 m together with the Appendix (A) natural gas properties indicates an $\approx$ 2% change in pressure across the height of the reservoir; allowing a constant reservoir pressure

assumed for all elements with sufficient accuracy.

$$\rho = \frac{P}{ZRT} \tag{10}$$

$$P_h = \rho g \Delta Z \tag{11}$$

$$\frac{P_h}{P} = \frac{g \Delta Z}{ZRT} \tag{12}$$

Where P_h is the hydrostatic pressure; R the specific gas constant, T the temperature, ΔZ the reservoir thickness and Z the real gas compressibility factor.

3.3. Model Testing and Verification

3.3.1. Verification of The Pressure Solution

The above numerical model can be compared with the analytical Line Source pressure Solution (LSS) for an infinitely acting reservoir with a constant, laminar flow, production rate in a radial system (Al-Hussainy et al., 1966). Their solution uses pseudo-pressure, a term that combines the pressure, the viscosity and the gas compressibility, or Z-factor, into one equation (Eq. 13).

$$\psi = \int_{P_{ref}}^{P} \frac{2P}{\mu Z} dP \tag{13}$$

The solution by Al-Hussainy et al. (1966) is:

$$\psi = \psi_i + \frac{\psi_i Q_d}{2} Ei\left(-\frac{\phi \mu C_t r^2}{4 \lambda k t}\right) \tag{14}$$

$$Q_d = \frac{\Gamma T Q_{sc}}{kh\psi_i} \tag{15}$$

Where: Q_d is the dimensionless rate, Γ is a constant multiplication factor, k is the permeability, h is the reservoir thickness and ψ_i is the pseudo-pressure at initial reservoir conditions. Fig. 4 is a comparison of the numerical and analytical solutions for the model parameters described in Appendix C. A close match

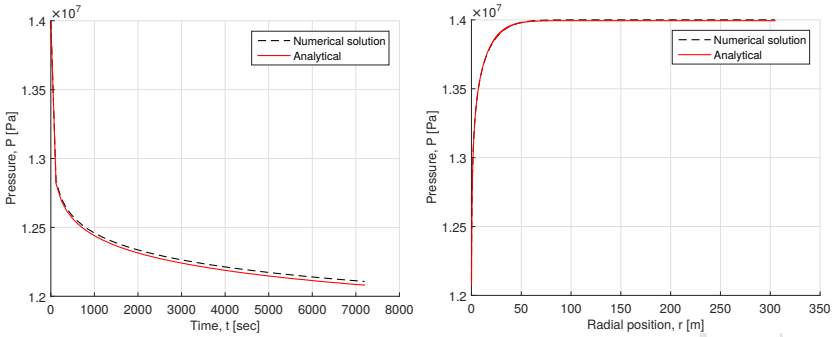

Figure 4: Plot of numerical and analytical solution. *left* Transient wellbore pressure, *right* Radial reservoir pressure

is observed for both the radial pressure distribution and the transient wellbore pressures. The reservoir temperature decreases as the well starts producing at a constant mass flow rate of gas (Fig. 5). This is due to (1) the cooling due to transient gas expansion (a dominant effect initially that quickly disappears, as confirmed by our analytical solution) and (2) the Joule-Thomson cooling (a nearly constant effect that acts as a non-uniformly distributed heat sink). Heat conduction, as will be discussed later, is negligible compared to heat convection.

3.3.2. Verification that the Mesh Refinement and Time Step Size are Sufficient

Figs. 5 and 6 illustrate the sensitivity of the numerical solution to the size of the time step and the mesh (using the case study described in Appendix C). As expected, the mesh size had the greatest effect on the solution accuracy. This occurs because the solver automatically adjusts the time step to ensure convergence.

Table 1: Effect of time step on simulation time

Time step (seconds)	1	30	60	120
Simulation time (seconds)	34,171	3,154	2,309	1,233

The solutions converge as the number of mesh elements increase (Fig. 6). We selected the mesh size and time steps corresponding to the converging cases,

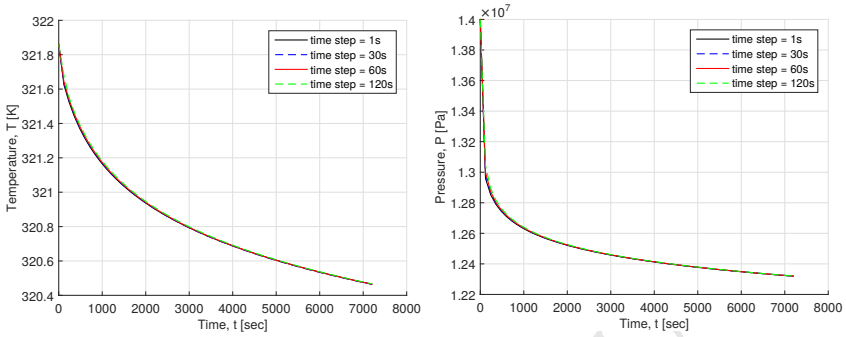

Figure 5: Plot of wellbore pressure and temperature for different time-step size. *left* Transient wellbore temperature, *right* Transient wellbore pressure

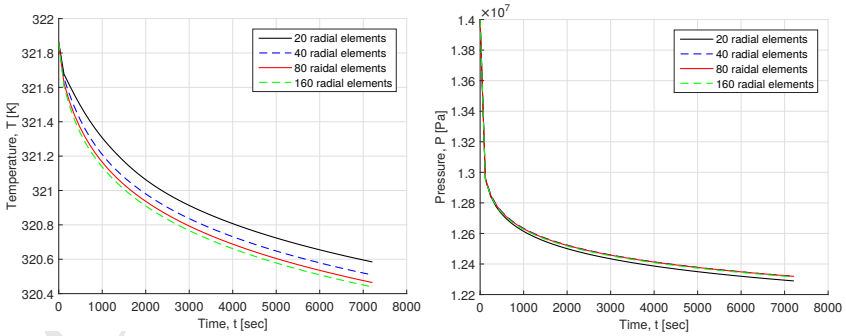

Figure 6: Plot of wellbore pressure and temperature for different number of elements. *left* Transient wellbore temperature, *right* Transient wellbore pressure

Table 2: Effect of element size (or number of elements) on simulation time

Radial elemets	20	40	80	160
Simulation time (seconds)	360	2,857	33,416	133,116

namely: the mesh with 80 radial elements and a time step of 1 second.

4. Analytical Modelling

Knowledge of the pressure distribution in the zone of interest is required when using Eq. 5 to develop an analytical solution. Developing this analytical solution requires a number of assumptions and a combination of numerical simulations and existing solutions. The case study described in Appendix C is used to study and validate the derived analytical solution.

4.1. Assumptions Made in the Analytical Model

The following observations made it possible to simplify the thermal model sufficiently to obtain an asymptotic solution for the temperature at early times.

4.1.1. Temperature Independence of the Pressure Solution

The assumption that small temperature change does not significantly affect the pressure solution was confirmed by comparing the solution of the combined pressure and temperature equations and the equivalent pressure solution at a constant temperature. Very little pressure difference ($\approx 0.2\%$ in Fig. 7) is observed between the two solutions.

Similarly, the variation in the pseudo-pressure for a natural gas can be shown to be negligible (Figure 8) by considering the effect of the relatively small temperature change. It is expected that changes in the pressure solution will also be negligible since it can also be expressed as a function of pseudo-pressure. We can therefore reasonably conclude that it is not necessary to account for the effect of temperature change when using the existing pressure solution in the thermal

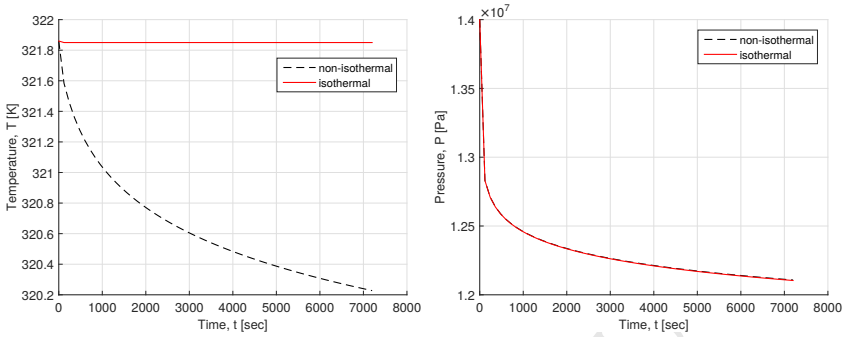

Figure 7: Plot of wellbore pressure and temperature for isothermal and non-isothermal conditions. *left* Transient wellbore temperature, *right* Transient wellbore pressure

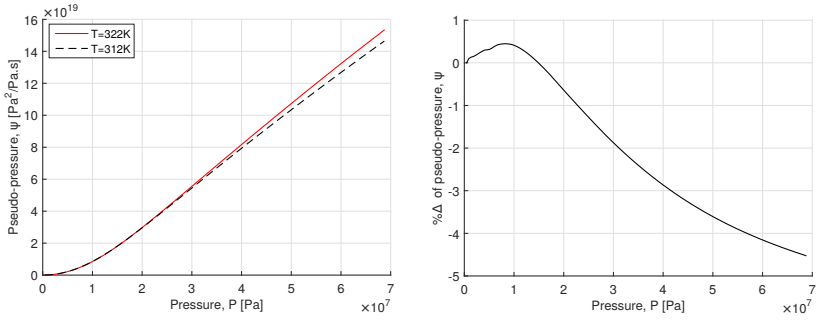

Figure 8: *left* Plot of pseudo-pressure against pressure. *right* Plot of change in pseudo-pressure for $\Delta T \approx 10K$

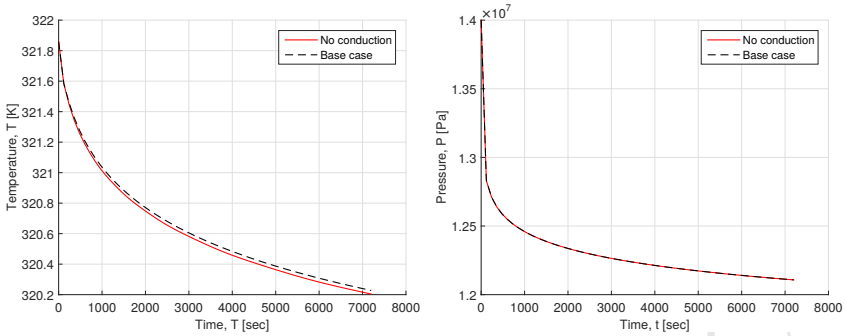

Figure 9: Plot of wellbore pressure and temperature for base case and case without conduction effects. *left* Transient wellbore temperature, *right* Transient wellbore pressure

model for such relatively small formation temperature changes. This assumption simplifies the problems solution by allowing the pressure to be decoupled from the temperature.

4.1.2. The Negligible Effect of Heat Conduction

The observation that heat conduction has very little effect on transient temperature at early times has also been verified numerically (Fig. 9) by comparing simulations which included and neglected the thermal conductivity. The contribution of heat conduction to the transient temperature response at early times was found to be small ($< 4\%$ with a maximum temperature change of 0.03K). It also had virtually no effect on the pressure response. Conduction can thus be neglected without significantly affecting the accuracy of the solution. This has also been observed in the other TTA studies.

Eqn. 16 simplifies the thermal model by eliminating the conduction term:

$$\begin{aligned} \overline{\rho C_p}\frac{\partial T}{\partial t} - \phi\beta T\frac{\partial P}{\partial t} - \phi C_f\left(P + \rho_r C_{pr} T\right)\frac{\partial P}{\partial t} \\ = -\rho \boldsymbol{v} C_P \cdot \nabla T + \beta T \boldsymbol{v} \cdot \nabla P - \boldsymbol{v} \cdot \nabla P \end{aligned} \tag{16}$$

N.B. App and Yoshioka (2013) showed that, when the Peclet number approaches zero, the conduction effect can become dominant. An example is a tight, very low permeability, formation with the low flow velocities. For produc-

tion from conventional reservoirs (similar to what is being studied) the Peclet number is usually high enough to ignore conduction effects.

4.2. Identification of the Values of the Constant Parameters in Eq. 16

The value of some of the coefficients in the simplified thermal model (with conduction eliminated) has been investigated by modelling a one-dimensional, radial system with a constant production rate and infinite acting boundaries. Eq. 16 can be written in a different form:

$$K1\frac{\partial T}{\partial t} - K2\frac{\partial P}{\partial t} = K3\frac{\partial P}{\partial r}\frac{\partial T}{\partial r} - K4\frac{\partial P}{\partial t}^2 \tag{17}$$

The coefficients K1, K2, K3 and K4 can be defined by comparing Eq. 17 with Eq. 16:

$$K1 = \overline{\rho C_p} = \phi\rho C_p + (1-\phi)\,\rho_r C_{pr} \tag{18}$$

$$K2 = \phi\beta T + \phi C_f\,(P + \rho_r C_{pr} T) \tag{19}$$

$$K3 = \frac{\rho C_P k}{\mu} \tag{20}$$

$$K4 = \frac{(\beta T - 1)\,k}{\mu} \tag{21}$$

The values of K1, K2, K3 and K4 may be calculated based on the numerical simulation results for the case considered. The relative change in the values of K1, K2, K3 and K4 over the pressure and temperature changes considered were 0.36%, 1.5%, 12.06% and 0.94% respectively. K1, K2 and K4 may be assumed to be constant, further simplifying the derivation of the analytical solutions.

4.3. Solution of the Simplified Thermal Model

4.3.1. Assumptions

The following assumptions were made in arriving at the early-time solution:

1. Conduction within the formation and heat exchange with the surround rocks effects are negligible.

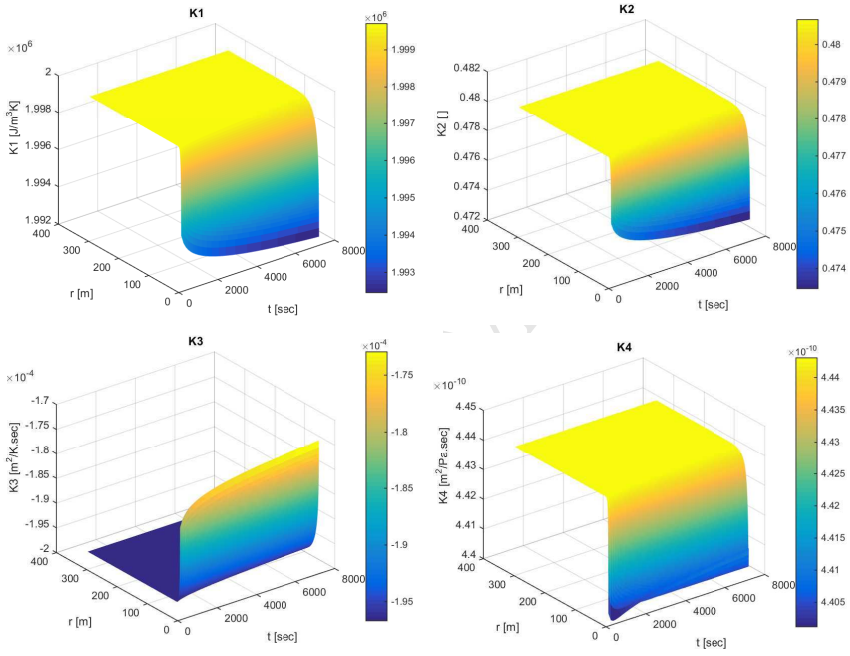

Figure 10: Plot of coefficients of Eq. 17

2. The existing Line Source Pressure Solution (at constant temperature) for gas flow in porous media can be used to calculate pressure.
3. The relationship between pressure and pseudo-pressure can be represented by a straight line. This is normally valid within the range of pressure between the initial reservoir pressure and the bottom hole flowing pressure (measured for the period of the analysis).
4. The term $\exp\left(-\frac{\phi\mu C_t r^2}{4\lambda k t}\right)$ can be assumed to equal unity for $r < 3 metres$ (a typical investigation distance in TTA) if very early times ($t < 0.5 hrs$) are excluded. This is shown graphically in Fig. 12.

$$\exp\left(-\frac{\phi\mu C_t r^2}{4\lambda k t}\right) = \exp\left(-\frac{\alpha r^2}{t}\right) \approx 1$$

5. Non-Darcy effects are neglected.
6. There is instantaneous thermal equilibrium between the rock and the flowing fluid.

Further assumptions about the gas properties are as follows;

7. The reservoir and well temperature are always higher than the critical temperature of the gas and below the Joule-Thomson inversion temperature.
8. The gas behaviour can be adequately modelled using the real gas compressibility factor (z-factor).

The following assumptions are required when using the line source, pressure solution Ahmed (2001):

9. The reservoir is infinitely acting.
10. The well is producing at a constant flow rate.
11. The wellbore is situated at the centre of the reservoir.

4.3.2. Solution Method

1. A linear relationship between pressure and pseudo-pressure was derived. This was obtained for a specific gas by calculating the gradient (or fitting a straight line) of the pressure pseudo-pressure curve between the value at

the initial reservoir pressure and the lowest expected flowing bottom-hole pressure. This relationship can be obtained from the gas PVT data or by using appropriate correlations.

$$P = A + B\psi \tag{22}$$

$$\frac{dP}{d\psi} = B \tag{23}$$

The above relationship was derived around the initial temperature and pressure of the reservoir, as required by our thermal model. This relationship, determined from Fig. 2-4 of ERCB (1979), enables us to convert the pseudo-pressure solution to the pressure. Fig. 11 is the plot of the pressure versus the pseudo-pressure. There is an approximately linear correlation between these two parameters in the area of interest indicated (indicated by a red box).

$A = 6 \times 10^{6}[Pa]$

$B = 0.5 \times 10^{-12}[Pa/(Pa^2/Pa.s)]$

where ψ is the pseudo-pressure in $[Pa^2/Pa.s]$ and P is the pressure in $[Pa]$.

The pressure drawdown satisfies the Darcy assumption when there is a linear relationship between pressure and pseudo-pressure for all values and at all times between the bottom-hole pressure and the reservoir pressure.

2. Using the existing Line Source Pressure Solution (LSS) for gas flow in porous media:

$$\psi = \psi_i + \frac{\psi_i Q_d}{2} Ei\left(-\frac{\phi\mu C_t r^2}{4\lambda k t}\right) \tag{24}$$

$$\begin{aligned}\frac{d\psi}{dr} &= \frac{\psi_i Q_d}{2}\left[\frac{\exp\left(-\frac{\phi\mu C_t r^2}{4\lambda k t}\right)}{\left(\frac{\phi\mu C_t r^2}{4\lambda k t}\right)}\right]\left(\frac{2\phi\mu C_t r}{4\lambda k t}\right) \\ &= \psi_i Q_d\left[\frac{\exp\left(-\frac{\phi\mu C_t r^2}{4\lambda k t}\right)}{r}\right]\end{aligned} \tag{25}$$

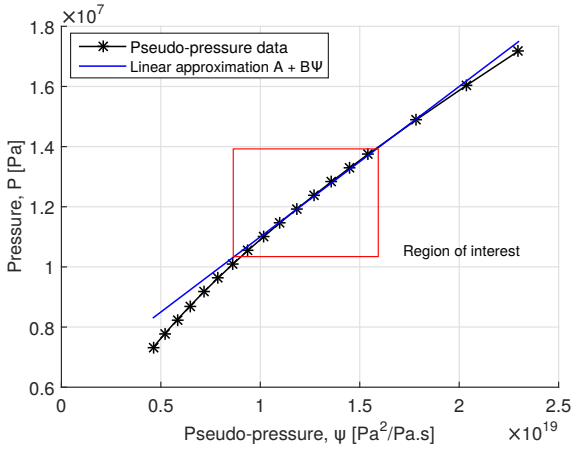

Figure 11: Plot showing linear approximation of pressure pseudo-pressure relationship

$$\frac{d\psi}{dt} = \frac{\psi_i Q_d}{2}\left[\frac{\exp\left(-\frac{\phi\mu C_t r^2}{4\lambda k t}\right)}{\left(\frac{\phi\mu C_t r^2}{4\lambda k t}\right)}\right]\left(-\frac{\phi\mu C_t r^2}{4\lambda k t^2}\right) = -\frac{\psi_i Q_d}{2}\left[\frac{\exp\left(-\frac{\phi\mu C_t r^2}{4\lambda k t}\right)}{t}\right] \tag{26}$$

The solution for pressure as a function of radial position and time is obtained by combining the relationship between the pressure and the pseudo-pressure as described above:

$$P = A + B\left[\psi_i + \frac{\psi_i Q_d}{2} Ei\left(-\frac{\phi\mu C_t r^2}{4\lambda k t}\right)\right] \tag{27}$$

$$\frac{dP}{dr} = B\psi_i Q_d\left[\frac{\exp\left(-\frac{\phi\mu C_t r^2}{4\lambda k t}\right)}{r}\right] \tag{28}$$

$$\frac{dP}{dt} = -\frac{B\psi_i Q_d}{2}\left[\frac{\exp\left(-\frac{\phi\mu C_t r^2}{4\lambda k t}\right)}{t}\right] \tag{29}$$

3. Excluding early times ($t < 0.5hr$) and investigating near-wellbore zone ($r < 3m$) gives:

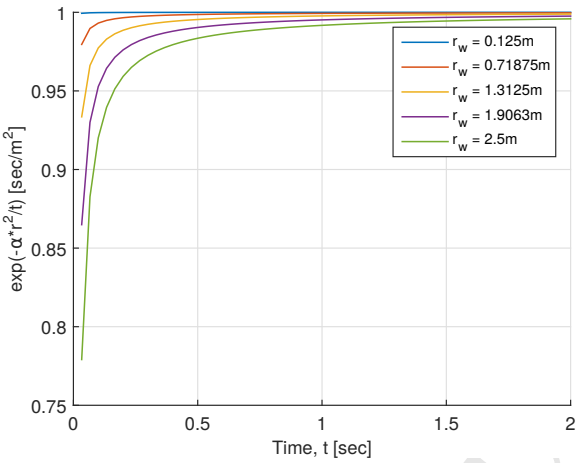

Figure 12: Plot of $\exp\left(-\frac{\alpha r^2}{t}\right)$ showing approximation to unity

$$\exp\left(-\frac{\phi\mu C_t r^2}{4\lambda k t}\right) = \exp\left(-\frac{\alpha r^2}{t}\right) \approx 1$$

$$\alpha = \frac{\phi\mu C_t}{4\lambda k} = 4.84182 sec/m^2$$

$$\frac{dP}{dr} = B\frac{\psi_i Q_d}{r} \tag{30}$$

$$\frac{dP}{dt} = -B\frac{\psi_i Q_d}{2t} \tag{31}$$

The assumption $\exp\left(-\frac{\alpha r^2}{t}\right) \approx 1$ gives a result equivalent to the log approximation of the line source solution for pressure.

4. Note that $\frac{dP}{dr} \propto \frac{1}{r}$ has similar characteristics to the equation derived by Ramazanov et al. (2010) for the transient wellbore temperature solution for oil production. Details of this derivation are given in Appendix B.

$$T_{wb}(t) = T_i + \varepsilon\left[P_{(r=r_T)} - P_{wf}(t)\right] + \eta^* \int_0^t \frac{dP}{d\tau}_{r=r_T} d\tau \tag{32}$$

The transient expansion term for gas, which is represented by the third term in Eqn. (32), can be redefined using the $\frac{dP}{dt}$ term obtained from the

LSS. The $\frac{dP}{dt}$ term is given by:

$$\frac{dP}{dt} = -B\frac{\psi_i Q_d}{2}\left[\frac{\exp\left(-\frac{\alpha r^2}{t}\right)}{t}\right] \tag{33}$$

Therefore the integral in the third term of the solution given in Eq. 32 is:

$$\int_0^t \frac{dP}{d\tau}_{r=r_T} d\tau = \int_0^t -B\frac{\psi_i Q_d}{2}\left[\frac{\exp\left(\frac{-\alpha({r_w}^2+2U_o K1\cdot\tau)}{K1\cdot\tau}\right)}{\tau}\right] d\tau \tag{34}$$

Details of the integration is given in Appendix B

$$T_{wb}(t) = T_i + \varepsilon\left[P_{(r=r_T)} - P_{wf}(t)\right] + \eta^{**}\left[P_{wf}(t) - P_i\right] \tag{35}$$

Where:

$$r_T = \sqrt{({r_w}^2 + 2U_o t)}$$

$$\alpha = \frac{\phi\mu c}{4\lambda k}$$

$$Q_d = \frac{\Gamma T Q_{sc}}{kh\psi_i}$$

$$U_o = c\boldsymbol{v}(r,t)r$$

$$\boldsymbol{v}(r,t) = \frac{k}{\mu}\frac{dP}{dr}$$

$$c = \frac{C_p\rho}{C_t}$$

$$C_t = \overline{C_p\rho} = \phi C_p\rho + (1-\phi)\,C_{pr}\rho_r$$

$$\varepsilon = \frac{1-\beta_T T}{C_p\rho}$$

$$\eta^{**} = \eta^{*}\exp\left(-2\alpha U_o\right)$$

$$\eta^{*} = \phi c\eta$$

$$\eta = \frac{\beta_T T}{C_p\rho}$$

The exponential integral function can be represented using the logarithmic approximation for most practical cases. We can therefore represent $P_{(r=r_T)}$, $P_{wf}(t)$ and P_i as:

$$P_{(r=r_T)} = A + B\left(\psi_i + \frac{\psi_i Q_d}{2}\left[\gamma + \ln\left(\frac{\phi\mu C_t {r_T}^2}{4\lambda k t}\right)\right]\right) \tag{36}$$

$$P_{wf}(t) = A + B\left(\psi_i + \frac{\psi_i Q_d}{2}\left[\gamma + \ln\left(\frac{\phi\mu C_t {r_w}^2}{4\lambda k t}\right)\right]\right) \tag{37}$$

$$P_i = A + B\psi_i \tag{38}$$

Eq. 35 can now be written as shown below:

$$\begin{aligned} T_{wb}(t) = T_i + \varepsilon\left(B\frac{\psi_i Q_d}{2}\left[\ln\left(\frac{{r_T}^2}{{r_w}^2}\right)\right]\right) \\ +\eta^{**}\left(B\frac{\psi_i Q_d}{2}\left[\gamma + \ln\left(\frac{\phi\mu C_t {r_w}^2}{4\lambda k t}\right)\right]\right) \end{aligned} \tag{39}$$

Eq. 39 can be expressed explicitly as a function of time, as shown in Eq. 40

$$\begin{aligned} T_{wb}(t) = T_i + \frac{B\Gamma T Q_{sc}}{2kh}\left[\left(\frac{1-\beta_T T}{C_p\rho}\left[\ln\left(\frac{\left[{r_w}^2 + 2\left(\frac{C_p\rho B\Gamma T Q_{sc}}{\overline{\rho C_p}\mu h}\right)t\right]}{{r_w}^2}\right)\right]\right)\right] \\ +\frac{B\Gamma T Q_{sc}}{2kh}\left[\left(\frac{\phi\beta_T T}{\overline{\rho C_p}}\exp\left(-\frac{2\alpha C_p\rho B\Gamma T Q_{sc}}{\overline{\rho C_p}\mu h}\right)\left[\gamma + \ln\left(\frac{\phi\mu C_t {r_w}^2}{4\lambda k t}\right)\right]\right)\right] \end{aligned} \tag{40}$$

4.4. Comparison of Different Solution Methods with the Full Numerical Solution

Two analytical solutions have been investigated: (1) with and (2) without transient expansion effects. The case described in Appendix C was used to compare the full analytical solution with the numerical solution that had been solved using the finite volume method implemented in OpenFOAM.

Numerical:. Full numerical solution

Analytical1:. Current analytical solution with expansion term

$$T_{wb}(t) = T_i + \varepsilon\left[P_{(r=r_T)} - P_{wf}(t)\right] + \eta^{**}\left[P_{wf}(t) - P_i\right] \tag{41}$$

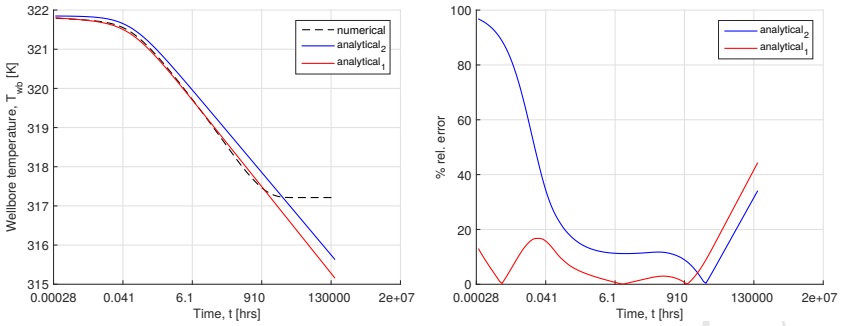

Figure 13: *left* Plot of transient wellbore temperature for numerical and analytical solutions. *right* Plot of percentage relative errors for the analytical solution methods

Analytical2:. Analytical solution without expansion term as used on the oil production studies by Ramazanov et al. (2010)

$$T_{wb}(t) = T_i + \varepsilon \left[P_{(r=r_T)} - P_{wf}(t)\right] \tag{42}$$

We obtained a close match between the *Analytical1* solution and the numerical results, while the *Analytical2* solution was significantly different. This indicates that neglecting the effect of transient expansion of gas on the sand-face temperature would significantly increase the error. Not surprisingly, an opposite conclusion for oil flow was made by Ramazanov et al. (2010).

Fig. 13 compares the three scenarios while Figure 13(b) shows the error between the analytical1 and numerical solution defined as:

$$\%Rel.Error = \frac{\sqrt{\left(\Delta T_{wb,analytical} - \Delta T_{wb,numerical}\right)^2}}{\Delta T_{wb,numerical}} \tag{43}$$

The analytical solution began to diverge from the numerical in the late time region. This is due to the reservoir boundary effect so that LSS no longer applies.

4.5. Sensitivity Analysis

4.5.1. Sensitivity to Gas Properties

An analysis was carried out to determine the sensitivity of the transient temperature response to changes in the properties of the gas (Table 3). The thermal expansion coefficient had the greatest effect on the predicted sand-face temperature. Hence a more precise value of the thermal expansion coefficient will lead to a more accurate estimation of the sand-face temperature.

Table 3: Sensitivity of transient temperature solution to variation in the properties of the gas

	% change in transient temperature due to a specified parameter			
% change in parameter	Viscosity	Thermal expansion coefficient	Specific heat capacity	Density
+50%	+13.0	-114.3	+19.3	+19.3
-50%	-23.7	+114.3	-42.2	-42.2

4.5.2. Appropriate Gas Property Estimation

It is important to determine the conditions at which the gas properties should be estimated since accurate gas property values have a considerable effect on the results.

1. The effect of temperature change may be neglected for the following reasons. Firstly, the temperature changes are small compared to pressure changes which we expect to be dominant. Further, we are deriving the temperature solution, hence it is logical to, at least initially, assume that the temperature change is an unknown in the analysis.
2. Three possible definitions of the pressure are the:
   (a) Initial reservoir pressure.
   (b) Stabilized bottom-hole pressure.
   (c) Volumetrically average reservoir pressure.

The stabilized pressure is the pressure at which (i) the radius of investigation equals the external reservoir radius or (ii) when the transient pressure effect is

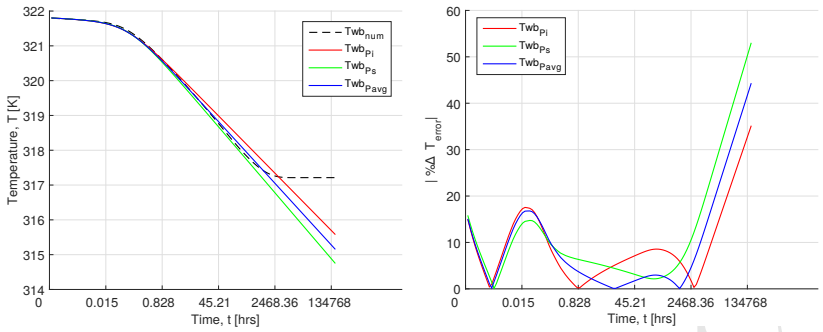

Figure 14: *left* Plot of analytical transient wellbore temperatures for three pressure conditions, *right* Plot of % relative errors of the analytical transient wellbore temperature for three pressure conditions

felt at the reservoir boundary ERCB (1979). The time required for stabilization can be determined from the equation $t_s = \frac{\phi\mu C_t r^2}{4\lambda k}$. It is about 121 hours for the case considered. The bottom-hole pressure at this time is about 11.4 MPa.

Table 4: Gas property values for simulation

Gas Properties	Initial pressure	Stabilized pressure	Average pressure	Units
Specific heat capacity	3111	2967	3041	J/kgK
Density	95.78	77.004	86.3737	kg/m^3
Viscosity	0.01515	0.01416	0.01465	cP
Thermal expansion coefficient	0.005198	0.004969	0.0051	K^-1

The average pressure is given by Eq. 44, while the errors are calculated using Eq. 45.

$$P_{avg} = \frac{P_i + P_s}{2} \tag{44}$$

$$\%Error = |\frac{\Delta T - \Delta T_{numerical}}{\Delta T_{numerical}}| \tag{45}$$

$$\Delta T = T - T_i; \Delta T_{numerical} = T_{numerical} - T_i$$

Fig. 14 indicates the errors associated with the volumetrically averaged properties are consistently lower than when the alternative definitions of the pressure are used. Hence the volumetrically averaged properties provide the closest match to the numerical solution for the case considered.

5. Limitations Due to Non-Darcy Effects

The analytical solution in this work was derived based on the assumption that the gas flow obeys Darcys law. However, it is well known that the gas flow deviates from Darcys law as flow velocity increases. Forchheimers equation, Eq. 46, describes this effect by adding an additional pressure drop term $\beta\rho|\boldsymbol{v}|\boldsymbol{v}$ (Wang and Economides, 2009) to Darcys equation that represents inertial effects.

$$-\nabla P = \frac{\mu}{k}\boldsymbol{v} + \beta\rho|\boldsymbol{v}|\boldsymbol{v} \tag{46}$$

A dimensionless number r_{nD} can be defined (Eq. 47) from Forchheimers equation. r_{nD} represents the ratio of the pressure gradients due to the non-Darcy and the Darcy effects.

$$r_{nD} = \frac{\beta\rho|\boldsymbol{v}|k}{\mu} \tag{47}$$

It is possible to estimate the velocities at which the non-Darcy effect is negligible (i.e. $r_{nD} \ll 1$). $r_{nD(crit)}$ can be defined as the critical non-Darcy ratio at which the pressure drops can be assumed to be mainly due to Darcy effects. It is therefore possible to obtain a corresponding critical flow velocity below which the non-Darcy effects can be neglected.

$$|\boldsymbol{v}_{(crit)}| = \frac{\mu r_{nDcrit}}{\beta\rho k} \tag{48}$$

Our analytical solution may thus be applied to velocities smaller than $\boldsymbol{v}_{(crit)}$. It is also possible to express this critical condition in terms of the surface

flowrates when the well geometry is known (i.e. well radius, r_w, and well length, L_w, are known) (Eq. 49).

$$Q_{sc(crit)} = \frac{\mu r_{nDcrit} 2\pi r_w L_w}{\beta \rho_{sc} k} \tag{49}$$

The limits of application of the analytical solution are determined by $Q_{sc(crit)}$ for a given well geometry and reservoir formation. This is calculated based on choosing a value of $r_{nD(crit)}$ at which the resulting errors are still acceptable. However, accurate estimation of $Q_{sc(crit)}$ depends on having a good knowledge of the value of β. Different correlations have been developed to estimate the value of the non-Darcy coefficient, some of which were published by Wang and Economides (2009).

Alternatively, the effect of non-Darcy flow on transient temperature can be investigated by considering the relationship between r_{nD} and the additional transient temperature drawdown due to non-Darcy flow.

$$r_{nD} = \frac{Q_{sc}\rho_{sc}\beta k}{2\pi r_W L_w \mu} \tag{50}$$

$$r_{nD} = \frac{Q_{sc}\rho_{sc}}{2\pi r_W L_w} \cdot \frac{\beta k}{\mu} \tag{51}$$

Where $\frac{Q_{sc}\rho_{sc}}{2\pi r_W L_w}$ is the mass flux at the well, β is usually expressed as a function of permeability k and porosity ϕ. The dimensionless number T_{nD} is the ratio of the additional temperature drawdown due to the non-Darcy flow effect to the temperature drawdown due to Darcy flow.

$$T_{nD} = \frac{T_{w(Darcy)} - T_{w(non-Darcy)}}{T_i - T_{w(Darcy)}} \tag{52}$$

Fig. 15 illustrates the effect of non-Darcy flow on the transient well temperature and pressure for the Appendix C case study. It clearly shows that the non-Darcy effect cannot always be neglected when applying the transient temperature solutions. Application of the analytical solutions with a reasonable accuracy therefore requires verification that the non-Darcy effects is negligible.

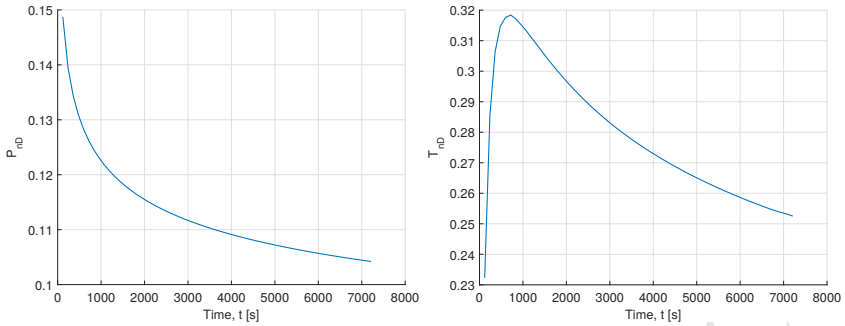

Figure 15: *left* Plot of ratio of non-Darcy to Darcy pressure drawdown. *right* Plot of ratio of non-Darcy to Darcy temperature drawdown

The values of T_{nD} for different values of r_{nD} were determined from numerical simulations (Fig. 16). The plots show that r_{nD} should be $< 10\%$ if the error in T_{nD} is to be $< 5\%$. Surface flowrates corresponding to this value of r_{nD} can be estimated and used as a guide when applying the analytical solution. N.B. The value of r_{nD} can be changed by changing the permeability k or the mass flux (or surface rate Q_{sc}) at the well. The curves of $r_{nD}(k)$ were obtained by changing the permeability from that of the base case, while the curves of $r_{nD}(Q)$ were obtained by changing the rate from that of the base case.

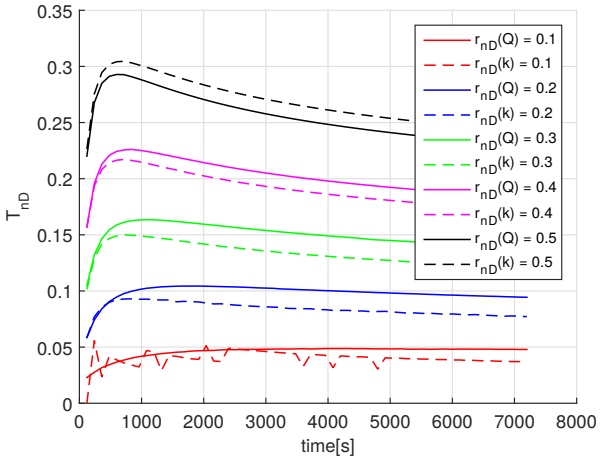

Figure 16: Curves of T_{nD} for different values r_{nD}

A better way of representing the critical surface flowrate is by expressing it as the rate per unit well-reservoir contact area. This term can then be applied to different well geometries and reservoir thicknesses.

$$Q_{scn(crit)} = \frac{Q_{sc(crit)}}{2\pi r_w L_w} = \frac{\mu r_{nD(crit)}}{\beta \rho_{sc} k} \tag{53}$$

6. Case Studies

The synthetic and real case studies presented below demonstrate the applicability of the analytical solution derived in this paper for calculating the transient, sandface temperature. The synthetic model is similar to the one used for validating the analytical solution in Section 4.4, but with different formation thickness, permeability and surface production rate values (Table 5). The real case is based on the downhole data measured in a gas production well in the Norwegian sector of the North Sea.

6.1. Synthetic Models

Three models are considered to compare the numerical and analytical solutions. Their formation thickness, permeability and surface production rates values are listed in Table 5. Full details for setting up each model are provided in Table 8 of Appendix D.

Table 5: Synthetic case study description

Property	Symbol	Unit	Case study 1	Case study 2	Case study 3
Formation thickness	h	m	30	30	60
Surface production rate	Q_{SC}	m^3/s	2.3	16.1	34.5
Permeability	k	$\times 10^{-15} m^2$	10	100	100

The prediction of the transient sandface temperature using the derived analytical solution (Eq. 40) was carried out for each case and compared with the accurate, numerical prediction. The results are shown in (Fig. 17, 18 & 19). The parameters used in the analytical equations are listed in Table 9 of Appendix D.

As can be seen, for the initial, infinitely-acting reservoir time period (i.e until the model boundary effects manifest themselves by causing the pressure and temperature to stabilise) the numerical and analytical predictions match very well in all three cases.

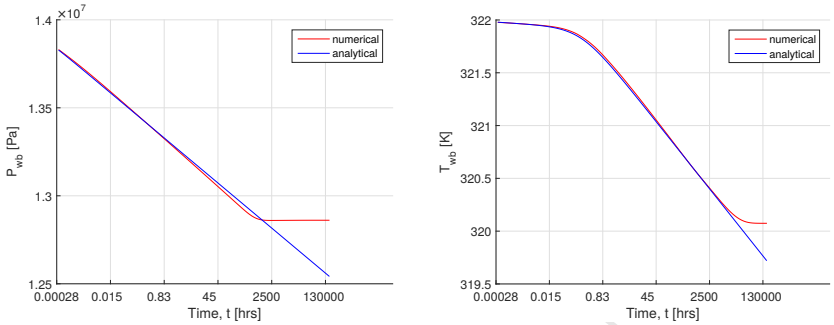

Figure 17: Case Study 1: *left* Plot of transient wellbore pressure . *right* Plot of transient wellbore temperature

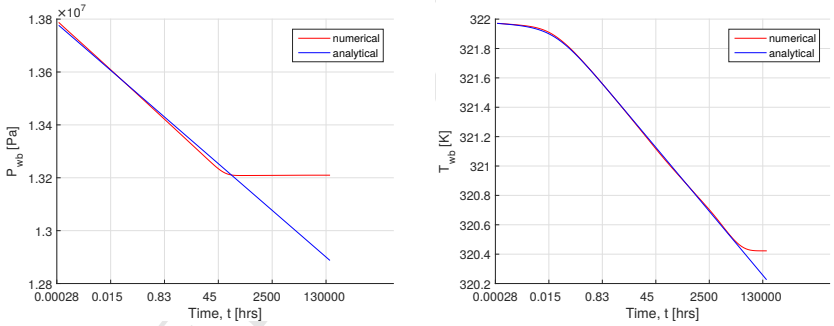

Figure 18: Case Study 2: *left* Plot of transient wellbore pressure . *right* Plot of transient wellbore temperature

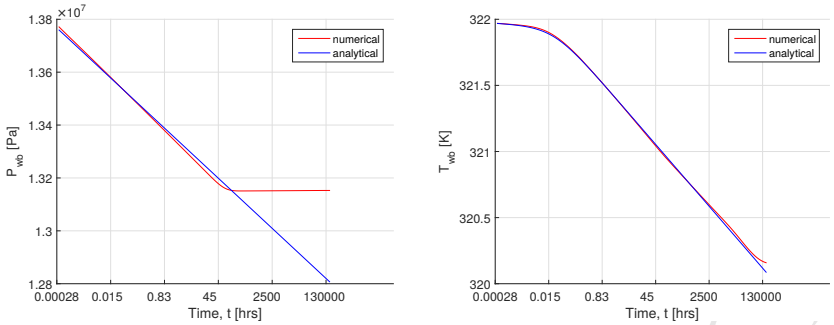

Figure 19: Case Study 3: *left* Plot of transient wellbore pressure . *right* Plot of transient wellbore temperature

6.2. Real Well Case Study

The data presented in this section were measured downhole in a vertical, gas producing well. Table 10 of Appendix D lists the fluid and formation properties. Fig. 20 shows the well rate and pressure data. The drawdown events (highlighted by red dots) are used in this section. This case study is presented and analysed in detail in Dada et al. (2016).

Pressure Transinet Analysis of the Build-up test was inconclusive, presumably becuase the well shut-in was not perfect. Rate Transient Analysis of the draw-down period has resulted in the estimate of the reservoir permeability*thickness product kh of 40,900 $mD.ft$ [$1.23 \times 10^{-11} m^3$]. Using this value in our analytical solution (Eq. 40) we are able to predict the transient temperature in the steadily declining temperature region (Fig. 21). As can be seen, the predicted and real temperature data match reasonably well. We were unable to model the very early period (first 6 hours) because of the well gradual opening and clean-up effects masking the pure sandface temperature response. The work to tackle these effects is ongoing.

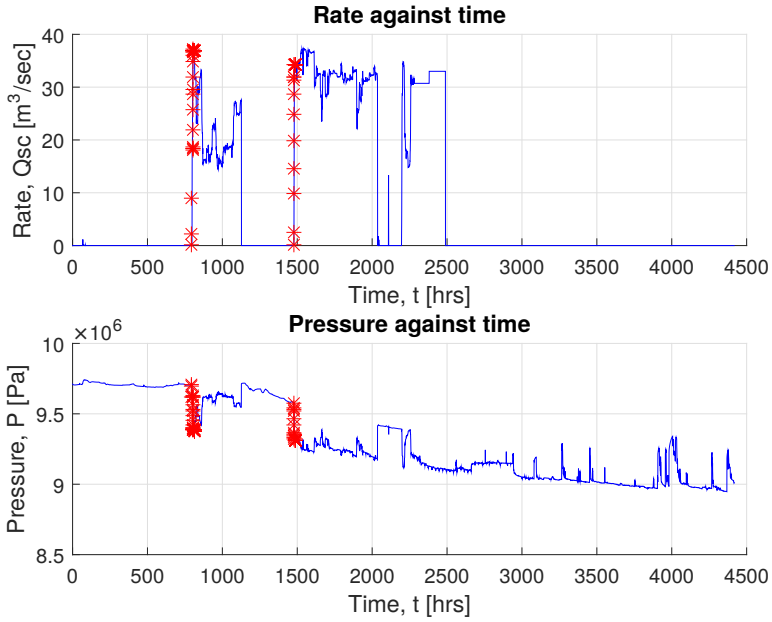

Figure 20: Real Well Case Study: Plot of surface rate and pressure

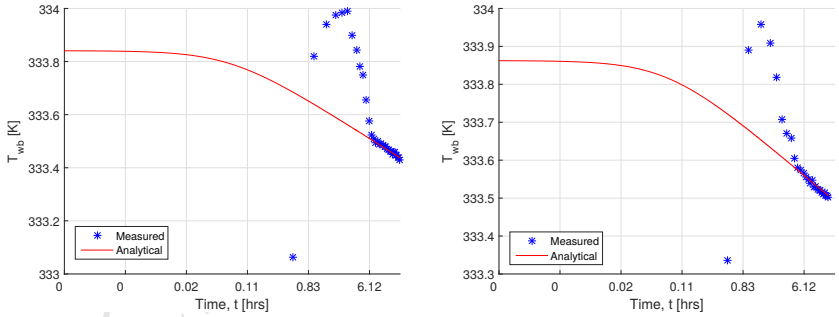

Figure 21: Real Well Case Study: *left* Plot of transient wellbore temperature for drawdown 1. *right* Plot of transient wellbore temperature for drawdown 2

7. Conclusions

Transient temperature data from producing wells can be invaluable for analysis and monitoring purposes. Robust models need to be available for analysis

and interpretation; these models should be able to handle single and multiphase flows of liquids and gases. However, very little work has been published on TTA for gases, and in particular there seems to be no analytical model existing for this.

In this work we tried to fill the existing gap in the development of robust TTA methods by developing an analytical model which can be used to predict transient sandface temperature of gas producing wells, as these models can then be inverted for use in TTA. We validated the solution by comparing against numerical simulations and observed a close match at times prior to the pressure transient arriving at the reservoir boundary. The derivation method for the analytical solution was described, along with the necessary assumptions and simplifications.

We have also made recommendations on the pressure and temperature conditions to be used when estimating the gas properties to be used in the solution since the choice of these values affects the accuracy of the results. The limitations of this solution due to non-Darcy effects were discussed and recommendations made on where our solution is applicable. Finally, synthetic and real well case studies were presented to illustrate the application of the analytical solution derived.

8. Appendix

8.1. Appendix A: Gas Properties and Equations-Of-State

The properties of gas are strongly dependent on pressure and temperature. To properly model the transient temperature changes, this pressure-temperature dependence of its properties has to be taken into account. Correlations and EOS are normally used. Some of the traditionally used correlations are applied in this work to realistically capture the gas behaviour.

Density. For gases at high pressure the relationship between density, pressure and temperature is given as:

$$\rho = \frac{P}{ZRT} \tag{54}$$

where $Z = f(P,T)$ The Z-factor is used to capture the non-ideal behaviour of the gas as a function of pressure and temperature, and it also varies with the composition of the gas.

Z-Factor. Z-factor is usually determined experimentally, and correlations are developed based on fitting experimental data to equations. The Benedict Webb Rubin (BWR) EOS was used instead of correlations for simplicity and consistency, as the molal volume (determined from BWR EOS) was used in determining the thermal properties of the gas. The Z-factor estimated using BWR EOS was in close agreement with that from correlations by Dranchuk and Abou-Kassem (1975).

Molal Density. The molal volume of the gas was calculated using the BWR EOS, similar to Benedict et al. (1942), this is shown in Eq. 55 below. The equation can be solved iteratively to determine the molal density d . Newtons iteration method was used, and rapid convergence of the solution was achieved. The values of the parameters are as given in Benedict et al. (1942).

$$\begin{aligned} P = \left(B_o RT - A_o - \frac{C_o}{T^2}\right) d + (bRT - a)\, d^3 \\ + a\alpha d^6 + \frac{cd^3}{T^2}\left[(1+\gamma d^2)\exp(-\gamma d^2)\right] \end{aligned} \tag{55}$$

$$B_o = 0.0426000; A_o = 1.85500; C_o = 0.0225700 \times 10^6; b = 0.00338004$$

$$a = 0.0494000; \alpha = 0.000124359; c = 0.00254500 \times 10^6; \gamma = 0.0060000$$

Viscosity. The correlation used in this case is that of Carr et al. (1954).

Thermal-Expansion-Coefficient. The thermal expansion coefficient is given by:

$$\beta_T = \frac{1}{v}\left(\frac{\partial V}{\partial T}\right)_P \tag{56}$$

Using the cyclic relationship $\left(\frac{\partial P}{\partial T}\right)_v\left(\frac{\partial T}{\partial V}\right)_P\left(\frac{\partial V}{\partial P}\right)_T = -1$

$$\left(\frac{\partial V}{\partial T}\right)_P = -\frac{\left(\frac{\partial P}{\partial T}\right)_V}{\left(\frac{\partial P}{\partial V}\right)_T} \tag{57}$$

$$\beta_T = -\frac{1}{V}\frac{\left(\frac{\partial P}{\partial T}\right)_V}{\left(\frac{\partial P}{\partial V}\right)_T} \tag{58}$$

Where $\left(\frac{\partial P}{\partial T}\right)_V$ & $\left(\frac{\partial P}{\partial V}\right)_T$ can be determined from BWRs EOS.

Specific Heat Capacity. The specific heat capacity of natural gas is dependent on pressure and temperature. To determine the specific heat capacity, we need to determine the specific heat capacity at ideal conditions, (atmospheric pressure) then we calculate the heat capacity departure at the high pressure existing in the reservoir. The method used was similar to Abou-Kassem and Dranchuk (1982).

$$C_p = (C_p - C_v) + (C_v - C_{vo}) + C_{po} - R = (C_p - C_{po}) + C_{po} \tag{59}$$

$(C_p - C_{po})$ is the isobaric heat capacity departure for the real gas, C_v is the specific heat capacity at constant volume for the real gas, C_{vo} is the specific heat capacity at constant volume for the ideal gas, C_{po} is the specific heat capacity at constant pressure for the ideal gas.

$$(C_p - C_v) = -T\frac{\left(\frac{\partial P}{\partial T}\right)_V^{\,2}}{\left(\frac{\partial P}{\partial V}\right)_T} \tag{60}$$

$$\left(\frac{\partial C_v}{\partial V}\right)_T = T\left(\frac{\partial^2 P}{\partial T^2}\right)_V \tag{61}$$

The derivatives $\left(\frac{\partial P}{\partial T}\right)_V$, $\left(\frac{\partial P}{\partial V}\right)_T$ & $\left(\frac{\partial^2 P}{\partial T^2}\right)_V$ can be determined from the BWRs EOS. Integrating Eq. 61 gives.

$$C_v - C_{vo} = \int_{vo}^{v} T\left(\frac{\partial^2 P}{\partial T^2}\right)_V dV \tag{62}$$

Since $V = \frac{1}{d}$, where: V is the molal volume of the gas and d is the molal density. Therefore the BWRs EOS can be written as:

$$P = \left(B_o RT - A_o - \frac{C_o}{T^2}\right) V^{-}1 + (bRT - a) V^{-3} + a\alpha V^{-6} + \frac{cV^{-3}}{T^2}\left[(1 + \gamma V^{-2}) \exp(-\gamma V^{-2})\right] \tag{63}$$

The procedure for calculating the specific heat capacity of the real gas at elevated pressures and temperatures is described below.

1. Using the BWRs EOS, determine $\left(\frac{\partial P}{\partial T}\right)_V$, $\left(\frac{\partial P}{\partial V}\right)_T$ & $\left(\frac{\partial^2 P}{\partial T^2}\right)_V$
2. Determine $C_v - C_{vo} = \int_{vo}^{v} T \left(\frac{\partial^2 P}{\partial T^2}\right)_V dV$
3. Determine $(C_p - C_v) = -T \frac{\left(\frac{\partial P}{\partial T}\right)_V^2}{\left(\frac{\partial P}{\partial V}\right)_T}$
4. Determine C_{po} from correlations
5. Substitute $(C_p - C_v)$, $C_v - C_{vo}$ & C_{po} into Eq. 59.

The correlation used to determine C_{po} is taken from Reid et al. (1977). The ideal heat capacity of the hydrocarbon was calculated using Yonedas group contribution method (Yoneda, 1979), and then corrections were made for non-hydrocarbon components according to Eqn.(26, 27 & 28) of the work published by Sutton and Hamman (2009).

Joule-Thomson Coefficient. The equation for calculating the Joule-Thompson coefficient is derived from the definition of the Joule-Thomson coefficient.

$$\mu_{JT} = \left(\frac{\partial T}{\partial P}\right)_H \tag{64}$$

$$dH = \left(\frac{\partial H}{\partial T}\right)_P dT + \left(\frac{\partial H}{\partial P}\right)_T dP \tag{65}$$

But at constant enthalpy,

$$dH = \left(\frac{\partial H}{\partial T}\right)_P dT + \left(\frac{\partial H}{\partial P}\right)_T dP = 0 \tag{66}$$

Dividing through by dP and rearranging gives

$$\left(\frac{\partial T}{\partial P}\right)_H = -\frac{\left(\frac{\partial H}{\partial P}\right)_T}{\left(\frac{\partial H}{\partial T}\right)_P} \tag{67}$$

$$C_p = \left(\frac{\partial H}{\partial T}\right)_P \tag{68}$$

$$\mu_{JT} = -\frac{\left(\frac{\partial H}{\partial P}\right)_T}{C_p} \tag{69}$$

$$\left(\frac{\partial H}{\partial P}\right)_T = V - T\left(\frac{\partial V}{\partial T}\right)_P = V\left[1 - \frac{T}{V}\left(\frac{\partial V}{\partial T}\right)_P\right] \tag{70}$$

$$\frac{1}{V}\left(\frac{\partial V}{\partial T}\right)_P = \beta_T \tag{71}$$

$$\frac{\partial H}{\partial P}_T = V[1 - |\beta_T T] = \frac{1}{\rho}[1 - \beta_T T] \tag{72}$$

$$\mu_{JT} = \frac{\beta_T T - 1}{\rho C_p} \tag{73}$$

To determine the gas properties over the range of pressure and temperature in the reservoir, the following properties (Table 6) were used.

Table 6: Natural gas properties

Property	Symbol	Value	Unit
Pseudo critical temperature	T_{pc}	190.6	K
pseudo critical pressure	P_{pc}	4.6624×10^6	Pa
Thermal conductivity	K_T	1.7	W/mK
Molal specific heat capacity of natural gas sample at ideal conditions	Cp_o	33.8901	$J/mol.K$
Universal gas constant	$\tilde{R}$	8.3145	kJ/kgK
Specific gas constant	R	519.6563	J/kgK
Specific gravity of gas	$S.G_f$	0.605	Unit
Viscosity at initial reservoir pressure	μ_i	1.52×10^{-5}	$Pa.s$
Mass fraction of H2S in natural gas		0	
Mass fraction of CO2 in natural gas		0	
Mass fraction of N2 in natural gas		0	

455

8.2. Appendix B: Solution of Simplified Thermal Model

$$K1\frac{\partial T}{\partial t} - K2\frac{\partial P}{\partial t} = K3\frac{\partial P}{\partial r}\frac{\partial T}{\partial r} - K4\left(\frac{\partial P}{\partial t}\right)^2 \tag{74}$$

Comparing Eq. 16 with Eq. 74, the coefficient terms K1, K2, K3 and K4 are defined as follows:

$$K1 = \overline{\rho C_p} = \phi\rho C_p + (1-\phi)\,\rho_r C_{pr} \tag{75}$$

$$K2 = \phi\beta T + \phi C_f\,(P + \rho_r C_{pr} T) \tag{76}$$

$$K3 = \frac{\rho C_P k}{\mu} \tag{77}$$

$$K4 = \frac{(\beta T - 1)\,k}{\mu} \tag{78}$$

Eq. 74 can be expressed as Eq. 79 below

$$\frac{\partial T}{\partial t} - \frac{K3}{K1}\cdot\frac{\partial P}{\partial r}\cdot\frac{\partial T}{\partial r} = \frac{K2}{K1}\frac{\partial P}{\partial t} - \frac{K4}{K1}\left(\frac{\partial P}{\partial r}\right)^2 \tag{79}$$

Let $t = t(\tau)$ and $r = r(\tau)$

$$\frac{\partial t}{\partial \tau} = 1 \tag{80}$$

$$\frac{\partial r}{\partial \tau} = -\frac{K3}{K1}\frac{\partial P}{\partial r} \tag{81}$$

Applying the method of characteristics, Eq. 79 can be written in the form below.

$$\frac{\partial T}{\partial t}\frac{\partial t}{\partial \tau} + \frac{\partial T}{\partial r}\frac{\partial r}{\partial \tau} = \frac{\partial T}{\partial \tau} = \frac{K2}{K1}\frac{\partial P}{\partial t} - \frac{K4}{K1}\left(\frac{\partial P}{\partial r}\right)^2 \tag{82}$$

Substitute Eq. 80 and 81) into Eq. 82

$$\frac{\partial T}{\partial \tau} = \frac{K2}{K1}\frac{\partial P}{\partial \tau} + \frac{K4}{K3}\frac{\partial P}{\partial \tau} \tag{83}$$

$$\frac{K2}{K1} = \frac{\phi\beta T + \phi C_f \left(P + \rho_r C_{pr} T\right)}{\overline{\rho C_p}}$$

But for most practical cases the formation compressibility can be assumed negligible, i.e.

$$\frac{K2}{K1} = \frac{\phi\beta T}{\overline{\rho C_p}} = \eta^*$$

$$\frac{K4}{K3} = \frac{(\beta T - 1)}{\rho C_p} = -\varepsilon$$

$$\frac{\partial T}{\partial \tau} = -\varepsilon \frac{\partial P}{\partial \tau} + \eta^* \frac{\partial P}{\partial \tau} \tag{84}$$

Eq. 84 is similar to that derived by Ramazanov et al. (2010), therefore it is possible to use a similar solution method as that used in their work.The solution was obtained by solving Eq. 84 along the characteristic of the problem (to be determined later). ;

$$T_{wb}(t) = T_i + \varepsilon \left[P_{(r=r_T)} - P_{wf}(t)\right] + \eta^* \int_0^t \frac{dP}{d\tau}_{r=r_T} d\tau \tag{85}$$

Next we consider the characteristic of this problem, by solving Eq. 80 and 81. Integrating Eq. 80 gives the following result.

$$t = \tau + C_1 \tag{86}$$

But $\frac{dP}{dr} = \frac{B\psi_i Q_d}{r}$, therefore $\frac{\partial r}{\partial \tau} = -\frac{K3 B\psi_i Q_d}{K1 r}$, integration of this gives

$$\frac{K1 r^2}{2K3 B\psi_i Q_d} = -\tau + C_2 \tag{87}$$

Applying the following boundary conditions; $t(0) = 0$ and $r(0) = s$ we can obtain $t = t(\tau, s)$ and $r = r(\tau, s)$

$$t = \tau \tag{88}$$

$$r^2 = -\frac{2 \cdot K3 \cdot B\psi_i Q_d t}{K1} + s^2 \tag{89}$$

Which can also be expressed as $\tau = \tau(t, r)$ and $s = s(t, r)$, τ and s are the characteristics of the problem.

$$\tau = t \tag{90}$$

$$s = \sqrt{r^2 + \frac{2 \cdot K3 \cdot B\psi_i Q_d t}{K1}} \tag{91}$$

Eq. 91 can be written in terms of U_o as defined by Ramazanov et al. (2010)

$$s = \sqrt{r^2 + 2U_o t} \tag{92}$$

Where $U_o = \frac{K3}{K1} \cdot B\psi_i Q_d = \frac{\rho C_p k}{\rho C_p \mu} \cdot r\frac{dP}{dr}$

From the characteristics obtained in Eq. 92 we have the same result as that defined by Ramazanov et al. (2010). Therefore we can safely use a similar solution as that obtained by Ramazanov et al. (2010).

$$s = r_T = \sqrt{{r_w}^2 + 2U_o t} \tag{93}$$

From Eq. 85 above, integration of the third term on the right hand can be carried out as follows:

$$\int_0^t \frac{dP}{d\tau}_{r=r_T} d\tau = \int_0^t -B\frac{\psi_i Q_d}{2}\left[\frac{\exp\left(\frac{-\alpha({r_w}^2+2U_o K1\tau)}{K1\tau}\right)}{\tau}\right] d\tau \tag{94}$$

$$\int_0^t \frac{dP}{d\tau}_{r=r_T} d\tau = -B\frac{\psi_i Q_d}{2}\int_0^t \left[\frac{\exp\left(\frac{-\alpha({r_w}^2+2U_o K1\tau)}{K1\tau}\right)}{\tau}\right] d\tau \tag{95}$$

$$\int_0^t \frac{dP}{d\tau}_{r=r_T} d\tau = -B\frac{\psi_i Q_d}{2}\exp(-2\alpha Uo)\int_0^t \left[\frac{\exp\left(\frac{-\alpha {r_w}^2}{K1\tau}\right)}{\tau}\right] d\tau \tag{96}$$

Let $\tau = 1/X$

$$\int_0^t \frac{dP}{d\tau}_{r=r_T} d\tau = -B\frac{\psi_i Q_d}{2}\exp(-2\alpha Uo)\left(-\int_{\frac{1}{t}}^{\infty}\left[\frac{\exp\left(\frac{-\alpha {r_w}^2 X}{K1}\right)}{X}\right] dX\right) \tag{97}$$

Let $Y = \frac{\alpha {r_w}^2 X}{K1}$

$$\int_0^t \frac{dP}{d\tau}_{r=r_T} d\tau = -B\frac{\psi_i Q_d}{2}\exp(-2\alpha Uo)\left(-\int_{\frac{\alpha {r_w}^2 X}{K1\tau}}^{\infty}\left[\frac{\exp(-Y)}{Y}\right] dY\right) \tag{98}$$

$$-\int_{\frac{\alpha {r_w}^2 X}{K1\tau}}^{\infty}\left[\frac{\exp\left(-Y\right)}{Y}\right]dY = Ei\left(\frac{-\alpha {r_w}^2}{K1\tau}\right) = Ei\left(\frac{-\alpha {r_w}^2}{t}\right)$$

$$\int_0^t \frac{dP}{d\tau}_{r=r_T} d\tau = -B\frac{\psi_i Q_d}{2}\exp(-2\alpha Uo)Ei\left(\frac{-\alpha {r_w}^2}{t}\right) \tag{99}$$

$$-B\frac{\psi_i Q_d}{2}Ei\left(\frac{-\alpha {r_w}^2}{t}\right) = P_{wf}(t) - P_i$$

$$T_{wb}(t) = T_i + \varepsilon\left[P_{(r=r_T)} - P_{wf}(t)\right] + \eta^*\exp(-2\alpha Uo)\left[P_{wf}(t) - P_i\right] \tag{100}$$

8.3. Appendix C: Case Study Definition

The case study used here describes a typical gas producing well and is taken from ERCB (1979)

Table 7: Case study for numerical simulation and analytical solutions

Property	Symbol	Value	Unit
Thermal conductivity	K_T	1.7	W/mK
Porosity	ϕ	0.15	
Specific heat capacity of gas	Cp_f	3030	J/kgK
Ratio of specific heat		1.31	
Specific gas constant	R	519.6563	J/kgK
Specific heat capacity of rock	Cp_r	920	J/kgK
Density of rock	ρ_r	2500	kg/m^3
Specific gravity of gas	$S.G$	0.605	
Pseudo-pressure at initial reservoir condition	ψ_i	16×10^{18}	$Pa^2/Pa.s$
Viscosity at initial reservoir pressure	μ_i	1.5×10^{-5}	$Pa.s$
Total formation compressibility at initial condition	Cf_i	8.724×10^{-8}	Pa^{-1}
Gas flow rate at standard conditions	Q_{SC}	2.3013	m^3/s
Pressure at standard conditions	P_{sc}	101325	Pa
Temperature at standard conditions	T_{sc}	289	K
Initial reservoir pressure	P_i	1.4×10^7	Pa
Initial reservoir temperature	T_i	322	K
Reservoir permeability	k	10×10^{-15}	m^2
Reservoir thickness	h	12	m
Well radius	r_w	0.125	m
Reservoir boundary radius	r_e	304.8	m
Thermal expansivity of gas	β_T	0.00522	K^{-1}
Constants in pressure solution	Γ	111.888	Pa/K
Constants in pressure solution	λ	1	

8.4. Appendix D: Case Study Data

Table 8: Application case studies

Property	Symbol	Value			Unit
Thermal conductivity	K_T	1.7			W/mK
Thermal conductivity	K_T	1.7			W/mK
Porosity	ϕ	0.15			
Specific heat capacity of gas	Cp_f	3030			J/kgK
Ratio of specific heat		1.31			
Specific gas constant	R	519.6563			J/kgK
Specific heat capacity of rock	Cp_r	920			J/kgK
Density of rock	ρ_r	2500			kg/m^3
Specific gravity of gas	$S.G$	0.605			
Pseudo-pressure at initial reservoir condition	ψ_i	16×10^{18}			$Pa^2/Pa.s$
Viscosity at initial reservoir pressure	μ_i	1.5×10^{-5}			$Pa.s$
Total formation compressibility at initial condition	Cf_i	8.724×10^{-8}			Pa^{-1}
Pressure at standard conditions	P_{sc}	101325			Pa
Temperature at standard conditions	T_{sc}	289			K
Initial reservoir pressure	P_i	1.4×10^7			Pa
Initial reservoir temperature	T_i	322			K
Well radius	r_w	0.125			m
Reservoir boundary radius	r_e	609.6			m
Thermal expansivity of gas	β_T	0.00522			K^{-1}
Constants in pressure solution	Γ	111.888			Pa/K
Constants in pressure solution	λ	1			
		Case study:			
		1	2	3	
Gas flow rate at standard conditions	Q_{SC}	2.3	16.1	34.5	m^3/s
Reservoir permeability	k	10	100	100	$\times 10^{-15} m^2$
Reservoir thickness	h	30	30	60	m

Table 9: Gas properties used to analytically model the 3 synthetic case studies described in Section 6.1

Property	Symbol	Case study 1	Case study 2	Case study 3	Unit
Stabilized pressure	P_{stab}	1.289	1.323	1.317	$\times 10^7 Pa$
Viscosity at average condition (i.e. $T_i, and P_{avg}$	μ_{avg}	1.491	1.497	1.495	$\times 10^{-5} Pa.s$
Density at average condition (i.e. $T_i, and P_{avg}$	ρ_{avg}	91.13	92.19	91.93	kg/m^3
Specific heat capacity at average condition (i.e. $T_i, and P_{avg}$	Cp_{avg}	3079	3087	3085	J/kgK
Thermal expansion coefficient at average condition (i.e. $T_i, and P_{avg}$	β_{Tavg}	5.161	5.173	5.170	$\times 10^{-3}/K$
Slope of pressure pseudo-pressure relationship	B	4.634	4.564	4.572	$\times 10^{-13} s$
Intercept of pressure pseudo-pressure relationship	A	6.561	6.675	6.660	$\times 10^6 Pa$

Table 10: Gas and formation properties used for analytical solution in real case study described in Section 6.2

Property	Symbol	value	Unit
Stabilized pressure	P_{stab}	9.379×10^6	Pa
Viscosity at average condition (i.e. $T_i, and P_{avg}$	μ_{avg}	1.373×10^{-5}	$Pa.s$
Specific gravity of gas	$S.G$	0.605	
Density at average condition (i.e. $T_i, and P_{avg}$	ρ_{avg}	60.73	kg/m^3
Specific heat capacity at average condition (i.e. $T_i, and P_{avg}$	Cp_{avg}	2840	J/kgK
Thermal expansion coefficient at average condition (i.e. $T_i, and P_{avg}$	β_{Tavg}	4.355×10^{-3}	$/K$
Specific heat capacity of rock	Cp_r	920	J/kgK
Density of rock	ρ_r	2500	kg/m^3
Slope of pressure pseudo-pressure relationship	B	5.0×10^{-13}	s
Intercept of pressure pseudo-pressure relationship	A	6.0×10^6	Pa

Acknowledgements

We wish to thank the sponsors of the "Value from Advanced Wells" Joint Industry Project at Heriot-Watt University, Edinburgh, United Kingdom for providing financial support for one of the authors.

References

Abou-Kassem, J.H., Dranchuk, P.M., 1982. Isobaric heat capacities of natural gases at elevated pressures and temperatures, in: SPE Annual Technical Conference and Exhibition, Society of Petroleum Engineers.

Ahmed, T., 2001. Reservoir Engineering Handbook. 2nd edn. ed., Gulf Professional Publishing.

Al-Hussainy, R., Ramey Jr, H.J., Crawford, P.B., 1966. The flow of real gases through porous media. journal of Petroleum Technology 18, 624–636.

App, J., Yoshioka, K., 2013. Impact of Reservoir Permeability on Flowing Sandface Temperatures: Dimensionless Analysis. SPE Journal 18, 685–694.

App, J.F., 2013. Influence of Hydraulic Fractures on Wellbore/Sandface Temperatures During Production, in: SPE Annual Technical Conference and Exhibition, Society of Petroleum Engineers.

Benedict, M., Webb, G.B., Rubin, L.C., 1942. An Empirical Equation for Thermodynamic Properties of Light Hydrocarbons and Their Mixtures II. Mixtures of Methane, Ethane, Propane, and n-Butane. The Journal of Chemical Physics 10, 747–758.

Bird, R.B., Lightfoot, E.N., Stewart, W.E., 2007. Transport Phenomena. John Wiley & Sons.

Carr, N.L., Kobayashi, R., Burrows, D.B., 1954. Viscosity of hydrocarbon gases under pressure. Journal of Petroleum Technology 6, 47–55.

Dada, A.O., Muradov, K.M., Davies, D.R., et al., 2016. Novel Solutions and Interpretation Methods for Transient, Sandface Temperature in Vertical, Dry Gas Producing Wells, in: SPE Intelligent Energy International Conference and Exhibition, Society of Petroleum Engineers.

Dranchuk, P.M., Abou-Kassem, H., 1975. Calculation of Z factors for natural gases using equations of state. Journal of Canadian Petroleum Technology 14.

Duru, O.O., Horne, R.N., 2010. Modeling reservoir temperature transients and reservoir-parameter estimation constrained to the model. SPE Reservoir Evaluation & Engineering 13, 873–883.

ERCB, 1979. Gas well testing - theory and practice. 4th edn. ed., Energy and Resource Conservation Boarf, E.R.C.B.

Geertsma, J., 1974. Estimating the coefficient of inertial resistance in fluid flow through porous media. Society of Petroleum Engineers Journal 14, 445–450.

Jasak, H., Jemcov, A., Tukovic, Z., 2007. OpenFOAM: A C++ library for complex physics simulations, in: International workshop on coupled methods in numerical dynamics, pp. 1–20.

Muradov, K., Davies, D., 2012a. Early-time asymptotic, analytical temperature solution for linear non-adiabatic flow of a slightly compressible fluid in a porous layer. Transport in porous media 91, 791–811.

Muradov, K., Davies, D., 2012b. Temperature transient analysis in horizontal wells: Application workflow, problems and advantages. Journal of Petroleum Science and Engineering 92, 11–23.

Muradov, K., Davies, D., 2013. Some Case Studies of Temperature and Pressure Transient Analysis in Horizontal, Multi-zone, Intelligent Wells, in: EAGE Annual Conference & Exhibition incorporating SPE Europec, Society of Petroleum Engineers.

OpenCFD, 2014. Openfoam user's guide. Version 2.3.0 ed., OpenFOAM Foundation.

Ramazanov, A., Valiullin, R.A., Shako, V., Pimenov, V., Sadretdinov, A., Fedorov, V., Belov, K., 2010. Thermal modeling for characterization of near wellbore zone and zonal allocation, in: SPE Russian Oil and Gas Conference and Exhibition, Society of Petroleum Engineers.

Reid, R.C., Prausnitz, J.M., Sherwood, T.K., 1977. The properties of gases and liquids. 4th ed.

Sui, W., Ehlig-Economides, C.A., Zhu, D., Hill, A.D., 2010. Determining multilayer formation properties from transient temperature and pressure measurements in comingled gas wells, in: International Oil and Gas Conference and Exhibition in China, Society of Petroleum Engineers.

Sui, W., Zhu, D., Hill, A.D., Ehlig-Economides, C., 2008. Model for transient temperature and pressure behavior in commingled vertical wells, in: SPE Russian Oil and Gas Technical Conference and Exhibition, Society of Petroleum Engineers.

Sutton, R.P., Hamman, J.G., 2009. Accuracy of fluid property estimates for calculating seismic properties, in: SPE Annual Technical Conference and Exhibition, Society of Petroleum Engineers.

Wang, X., Economides, M., 2009. Advanced natural gas engineering. Gulf Publishing Company.

Yoneda, Y., 1979. An estimation of the thermodynamic properties of organic compounds in the ideal gas state. I. Acyclic compounds and cyclic compounds with a ring of cyclopentane, cyclohexane, benzene, or naphthalene. Bulletin of the Chemical Society of Japan 52, 1297–1314.

- An analytical solution for predicting flowing sandface temperature is proposed.
- The analytical solution is sufficiently accurate with effect of conduction ignored.
- The appropriate condition for estimating the properties of the gas is also proposed.